Biogeosciences, 13, 873–885, 2016
www.biogeosciences.net/13/873/2016/
doi:10.5194/bg-13-873-2016

Biogeosciences Open Access EGU

The 2009–2010 step in atmospheric CO_2 interhemispheric difference

R. J. Francey and J. S. Frederiksen

CSIRO Oceans & Atmosphere, Aspendale, Victoria, Australia

Correspondence to: R. J. Francey (roger.francey@csiro.au)

Received: 6 August 2015 – Discussion started: 11 September 2015
Revised: 11 January 2016 – Accepted: 26 January 2016 – Published: 17 February 2016

Abstract. The annual average CO_2 difference between baseline data from Mauna Loa and the Southern Hemisphere increased by $\sim 0.8\,\mu mol\,mol^{-1}$ (0.8 ppm) between 2009 and 2010, a step unprecedented in over 50 years of reliable data. We find no evidence for coinciding, sufficiently large source and sink changes. A statistical anomaly is unlikely due to the highly systematic nature of the variation in observations. An explanation for the step, and the subsequent 5-year stability in this north–south difference, involves interhemispheric atmospheric exchange variation. The selected data describing this episode provide a critical test for studies that employ atmospheric transport models to interpret global carbon budgets and inform management of anthropogenic emissions.

1 Introduction

The record 2009–2010 increase in annual mean CO_2 difference between hemispheres, $\Delta C_{N\text{-}S}$, was reported by Francey et al. (2013) using data from Mauna Loa (mlo; 20° N, 156° W; altitude 3.4 km) and Cape Grim (cgo; 41° S, 145° E; 0.2 km) or the South Pole (spo, 90° S, 2.8 km). In the context of seeking an explanation for decadal differences between the fossil emission trends and trends in atmospheric CO_2 growth rate, Francey et al. (2013) attempted an empirical correction for reported natural influences on CO_2 growth using multiple regression of reported wild fires, volcanoes, and El Niño–Southern Oscillation (ENSO). None of these reported influences showed statistically significant anomalous behaviour in the 2009–2010 period.

A Commonwealth Scientific and Industrial Research Organisation (CSIRO) inversion, which deduces surface fluxes from atmospheric CO_2 observations, is based on atmospheric transport described by the Cubic Conformal Atmospheric Model (CCAM; McGregor and Dix, 2008). This explains the 2009–2010 ΔC with a 2010 Northern Hemisphere (NH) source in the Asian region, distributed widely enough to be unverifiable by "bottom-up" methods (R. Law, personal communication, 2015).

However, Poulter et al. (2014), using a terrestrial biogeochemical model, atmospheric carbon dioxide inversion, and global carbon budget accounting methods, suggested that the $\Delta C_{mlo\text{-}cgo}$ step might be explained by a record 2011 land carbon sink located in the semi-arid regions of the Southern Hemisphere (60 % of which was in Australia).

Furthermore, Patra (2015) demonstrated consistency in 2009–2010 between their ACTM (atmospheric chemistry transport model) simulations of $\Delta C_{mlo\text{-}cgo}$ and fluxes obtained from an inversion model. However, from the limited information available, it seems likely that both the $\Delta C_{mlo\text{-}cgo}$ and the inversion fluxes are dependent on the same transport parameterizations and so are not independent. Patra's comment prompts a question about the effectiveness of SF_6 measurements to "diagnose" model CO_2 interhemispheric transport.

In order to address the apparent conflicts, we update CO_2 measurements and search more widely for concurrence with independently determined parameters, including other trace gas species and atmosphere physical parameters influencing their distribution.

We are informed by a companion paper examining potential bias in the two largest terms in a global carbon budget (Francey et al., 2016). This documents significant reductions in susceptibility to bias in atmospheric CO_2 measurements since the 1990s and expresses concern about the spatial representation of reported CO_2 measurements, e.g. in monthly averaged data. Mismatch between the inversion model grid-scale and the scale of CO_2 representativeness at observing sites can introduce significant uncertainty in inversion mod-

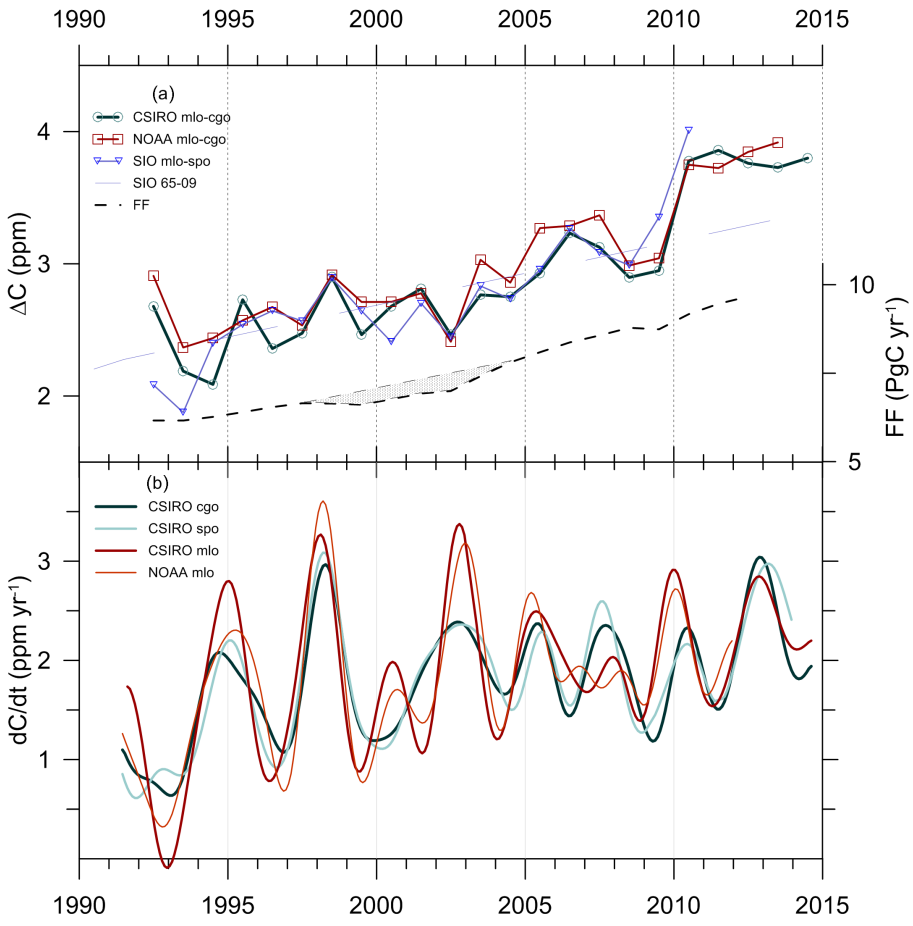

Figure 1. North–south differences and growth rates in CO_2 since 1990. Panel **(a)** shows, on the left axis, annual average (January–December) ΔC (ppm) from three programs – CSIRO, NOAA (mlo–cgo), and SIO (mlo–spo) – plotted mid-year. On the right axis are reported anthropogenic emissions (dashed line), with the correction suggested by Francey et al. (2013) (shaded), scaled so that the overall slope is similar to that from the long-term mlo–spo SIO record. Panel **(b)**: CSIRO (mlo, cgo, spo) and NOAA (mlo) growth rates, dC/dt, plotted mid- month. See the "Methods" section for details.

elling that may act to obscure large-scale systematic CO_2 behaviour.

2 Updated CO_2 data

Inversions of CO_2 data effectively interpret CO_2 spatial and temporal differences in terms of surface exchanges. Thus, Fig. 1 illustrates each type of difference, namely $\Delta C_{N\text{-}S}$ and dC/dt, in quality data with maximum spatial representation. Methods to obtain $\Delta\ C_{N\text{-}S}$ and dC/dt from monthly flask data are described in Appendix A.

The updated spatial comparisons of $\Delta C_{N\text{-}S}$ in Fig. 1a highlight the largely consistent results from the 1990s using data from flask samples collected and measured by the CSIRO, by the National Oceanic and Atmospheric Administration (NOAA; Dlugokencky et al., 2014) and by the Scripps Institution of Oceanography (SIO; Keeling et al., 2009) networks. For perspective, a comparison is also made with a linear regression through the SIO 5-decade $\Delta C_{mlo\text{-}spo}$ record. This shows an overall increase, generally attributed to the increase in fossil fuel (FF) emissions (Boden et al., 2013), which occur predominantly in the NH.

Annual global FF, including the correction suggested by Francey et al. (2013), are scaled and included to run parallel to the ΔC slope in Fig. 1a in order to emphasize the unusual magnitude of the 2009–2010 ΔC step. From this perspective the 0.8 ppm step, if it is the result of an anomalous flux, would equate to an annual 1.6 Pg C (NH) source, one sufficiently large and rapid that detection by bottom-up studies might be expected.

Also in Fig. 1a, the unusual post-2009 ΔC stability compared to the earlier record is obvious. Since methodologies have not significantly changed over this period, it suggests that measurement error is not a factor and the variability in the pre-2010 $\Delta C_{N\text{-}S}$ data is not random.

The temporal differences, dC/dt in Fig. 1b, show interannual variability on 3- to 5-year El Niño–Southern Oscil-

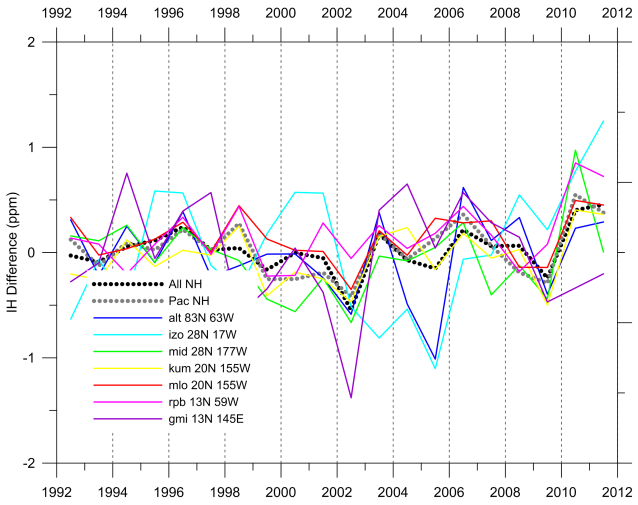

Figure 2. North–south CO_2 differences using other NH sites from the NOAA network: NH site minus cgo, using annual average baseline data (calendar year, plotted mid-year). Latitude and longitude of sites are provided in the legend.

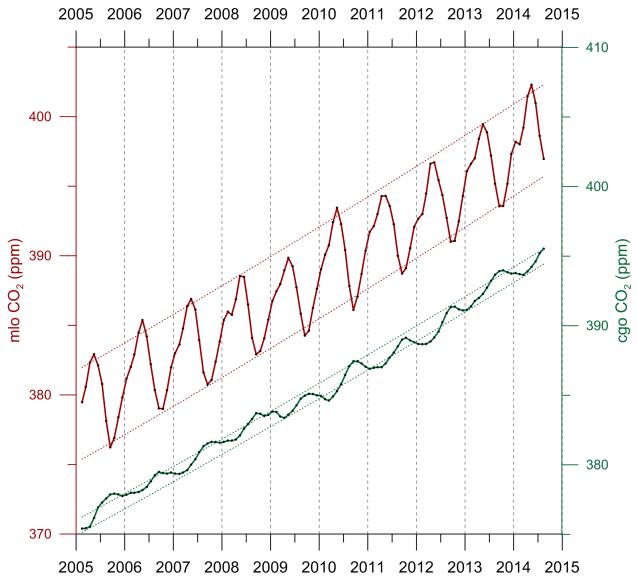

Figure 3. Monthly mlo and cgo CO_2 time series: CSIRO data of Fig. 1a are plotted monthly to better examine the onset of the 2009–2010 step (see text).

lation (ENSO) timescales. Using CCAM transport to invert CO_2 and $\delta^{13}CO_2$ observations, Rayner et al. (2008) concluded that interannual variability is forced primarily by climate variability on the equatorial land biosphere. This conclusion is consistent with the observation of limited influence on ΔC for equatorial exchanges in Fig. 1b, to be discussed further below. However, the question of the spatial representativeness of the selected CO_2 records is addressed first.

The hemispheric representativeness of baseline data from the mlo and cgo monitoring sites is supported by a study of aircraft vertical profiles at 12 global sites conducted in maximum convective conditions near midday (Stephens et al., 2007). The lower levels (< 1–2 km) of all 12 vertical profiles exhibited seasonal variation resulting from climate influence on regional surface carbon reservoirs. The amplitudes of the seasonal variation at mlo and cgo are the least in their respective hemispheres, which aids the definition of interannual variability at these sites.

While the spo data closely track cgo data, and other mid- to high-latitude Southern Hemisphere (SH) sites in the CSIRO network (Francey et al., 2013), the situation is less clear for mlo because of NH heterogeneity and proximity to Asia. A possible recent contributing factor at mlo may be the geographical susceptibility to rapidly increasing SE Asian pollution, "rapidly transported to the deep tropics" (Ashfold et al., 2015). In Fig. 2 we demonstrate similarity in year-to-year changes in ΔC using both Pacific and Atlantic extratropical NH sites from the NOAA network. The similarity is particularly significant in sign and magnitude for the two largest observed changes in 2009–2010 and 2002–2003, implying that especially for these periods, mlo represents NH behaviour.

During 2009–2010, dC/dt show a larger NH ENSO peak, leading that in the SH by around 6 months, a phase difference not observed for other significant El Niño peaks in Fig. 1b. This implies either an undetected NH source, or possibly, rapid changes in interhemispheric (IH) transport.

Poulter (2015) raises the issue of relative timing of the ΔC step and the response of SH savanna regions to the end of drought. To clarify this we include Fig. 3, showing CSIRO monthly baseline concentrations at mlo and cgo through the period. To aid discussion, the seasonal variations are compared to quadratic fits to the 1992–2014 data for each site, offset by $\pm$ the long-term amplitude of the seasonality: ± 3.3 ppm (6.6 ± 0.5 ppm peak-to-peak) at mlo and ± 0.55 ppm (1.10 ± 0.2 ppm p-p) at cgo.

There is a change in the mlo seasonality (the 2009 seasonal amplitude is the smallest and the 2010 amplitude the largest in this plot) between 2009 and 2010, which is of a sign and magnitude that most easily explains the 0.8 ppm step in annual average differences, $\Delta C_{\text{mlo-cgo}}$. Slightly lower CO_2 in the cgo baseline data in the 2010–2012 period could possibly be associated with an SH sink. However, the unusually large negative seasonal excursion from the mean, at the end of the 2009–2010 spring–summer uptake season, is before the October 2010 to March 2011 record floods in northern Australia which were identified as a trigger for the savanna response by Poulter et al. (2014); furthermore, the negative dip is followed by a near-average positive seasonal excursion in late 2010. Conventional descriptions of the Cape Grim seasonality have contributions from SH biosphere, seasonal SH ocean temperature changes, and ~6-month delayed NH biosphere signals (Law et al., 2006; Stephens et al., 2013); failure of a

delayed NH signal to reach Cape Grim might also contribute to low SH autumn CO_2 at Cape Grim. Nevertheless, a small contribution from an SH terrestrial sink is difficult to exclude in 2011 and 2012.

This question was further addressed at the 2014 Annual Cape Grim Science Meeting by Xingjie Lu, Ying-Ping Wang, and Rachel Law (Y.-P. Wang, R. Law, personal communications, 2014). They used the Community Atmosphere Biosphere Land Exchange model (CABLE; Law, 2014) to simulate net ecosystem production anomalies over the 2001 to 2012 period, finding SH anomalies that were mainly contributed by Argentina and Australia in 2010 and 2011. The timing of the terrestrial response of Lu, Wang and Law is similar to that of Poulter et al. (2014). Lu, Wang and Law investigated how the interannual variability in the CABLE biospheric fluxes affected $\Delta C_{mlo\text{-}cgo}$ using CO_2 response functions from the CCAM atmospheric model. When the CCAM CO_2 response functions are modified to represent baseline data (at cgo 20–30 % of time with strong winds over the Southern Ocean), this terrestrial signal is sufficiently diluted in the large well-mixed troposphere at mid-to-high southern latitudes to be reduced to insignificance in the reconstructed $\Delta C_{mlo\text{-}cgo}$. With their approval, the relevant CCAM modelling runs are included in the Supplement. This example highlights a requirement for high time resolution transport modelling coupled with similar resolution in the CO_2 data if such events are to be correctly attributed.

Finally, independent evidence for the NH origin of the 2009 to 2010 CO_2 ΔC step comes from a recent analysis of upper-troposphere measurements for 11 latitude bands between 30° N and 30° S (Matsueda et al., 2015) where the step is evident north of 10° N. These authors suggest a role for transport, as well as sources and sinks, to explain their year-to-year variations in latitudinal differences.

3 Responses in ΔC and dC/dt to other recent source and sink anomalies

Before examining a likely role of atmospheric transport in ΔC variations, we briefly examine Fig. 1 at the times of the major post-1992 independently documented anomalous CO_2 source and sink activity: the 1997–1998 Indonesian peat fires, the 2002–2003 NH drought and boreal wildfires, and the 2008 global financial crisis.

- The 1997–1998 Indonesian peat fires correspond to the largest El Niño peak dC/dt and were estimated as contributing around 1 Pg C (6.5 times the mean equatorial Asia emissions) to the atmosphere in 1997 (Page et al., 2009; Giglio et al., 2013). In Fig. 1 there is a small increase in $\Delta C_{N\text{-}S}$, with a barely significant larger NH dC/dt peak. A small response might be explained if the emissions are mixed into both hemispheres. The possibility that changes in IH mixing may also contribute to $\Delta C_{N\text{-}S}$ is discussed below.
- While the 2002–2003 $\Delta C_{N\text{-}S}$ in Fig. 1a is the second largest year-to-year increase (see also Fig. 2), it is also the largest difference in dC/dt between the hemispheres. Year 2003 corresponds to reductions in Europe's primary productivity which, according to Ciais et al. (2005), were "unprecedented during the last century" and released ~ 0.5 Pg C yr^{-1}. We add this to the 2003 Global Fire Emissions Database (GFED4) fire emissions in boreal America and boreal Asia of 0.31 Pg C, 2.5 times the 1997–2013 mean (Giglio et al., 2013). However, for emissions spread evenly over a full year, a relatively small ΔC impact is expected since the 2003 NH FF combustion was ~ 7.5 Pg C compared to < 0.7 Pg C from the non-FF sources.
- The global financial crisis (GFC) of 2007–2008 (Peters et al., 2012) coincides in Fig. 1b with the only occasion when the NH dC/dt ENSO peak is markedly smaller than that in the SH. While 2008 and 2009 are the two lowest global fire emission years in the GFED4 database, combined boreal emissions are near average, favouring the GFC as a more likely explanation for the dC/dt behaviour. However, it is less clear that relatively low 2008 and 2009 ΔC in Fig. 1a is attributable to the GFC, and a possible contribution from IH exchange is also examined below.

4 Anomalies in annual interhemispheric mixing

Meridional transport and eddy mixing due to large-scale eddy motions are sources of significant uncertainty in estimations of IH transport (Miyazaki et al., 2008). Here we examine the role of the opening and closing of the upper-tropospheric equatorial westerly duct, and associated interhemispheric Rossby wave propagation, as a contributor to the 2009–2010 $\Delta C_{mlo\text{-}cgo}$ shift, and other variations, shown in Fig. 1a.

Extratropical NH Rossby waves, including a branch of the Himalayan wave train, are able to penetrate into the SH when near-equatorial zonal winds are westerly in the upper-tropospheric duct centred on 140 to 170° W and 5° N to 5° S (Webster and Holton, 1982; Frederiksen and Webster, 1988; Webster and Chang, 1988). This region is delineated and its tropospheric relevance revealed in Fig. 4a, showing strongly correlated upper-tropospheric westerly winds with the Southern Oscillation Index (SOI) over the full 1949 to 2011 wind reanalysis data set (http://www.esrl.noaa.gov/psd/data/gridded/data.ncep.reanalysis.html).

The wind direction and strength (u_{duct}) in this duct are determined by seasonal and ENSO sea-surface temperature variations; the upper-troposphere westerlies are strongest in boreal winter and during La Niña periods, when they are correlated with proportional increases in near-equatorial transient kinetic energy (Fig. 6, Frederiksen and Webster, 1988),

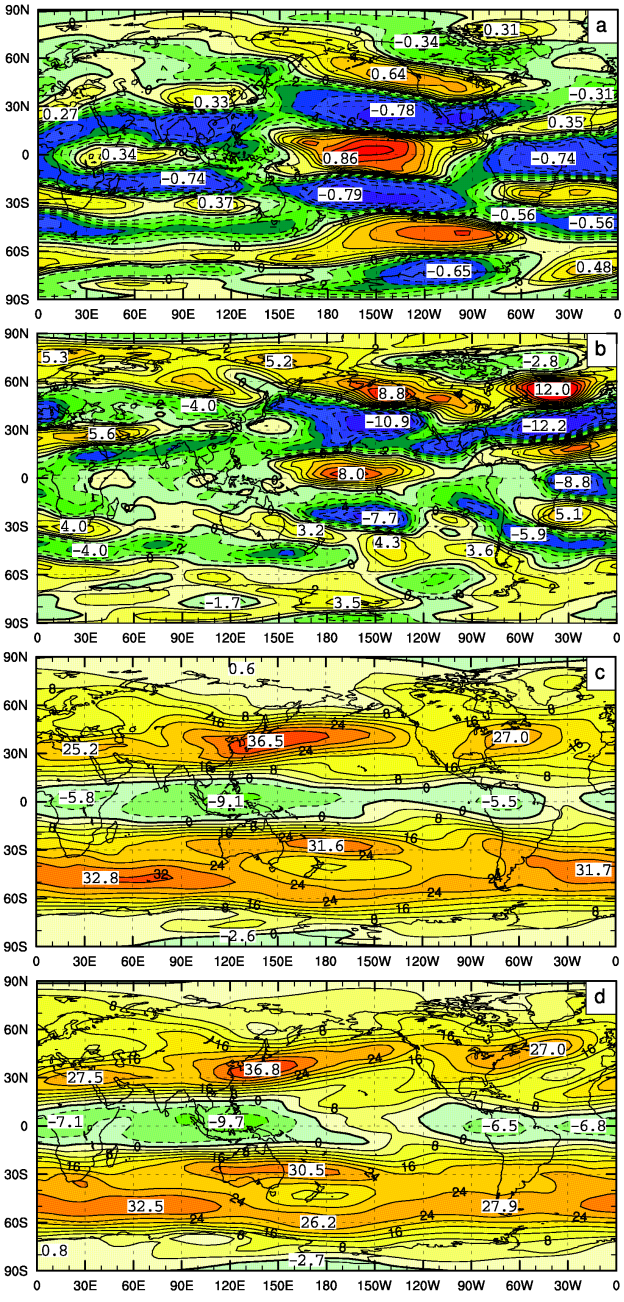

Figure 4. The equatorial upper-troposphere duct. Panel **(a)**: correlation over the annual cycle of 1949–2011 upper-tropospheric winds (300 hPa) with the Southern Oscillation Index (SOI), with strongest correlation in the equatorial Pacific duct. Panel **(b)**: the difference between open and closed equatorial duct patterns of Fig. 4d and c, showing similarity to the long-term correlation pattern in Fig. 4a. Panel **(c)**: July 2009 to June 2010 "closed-duct" pattern with 300 hPa easterly zonal wind in the equatorial duct. Panel **(d)**: July 2008 to June 2009 "open-duct" pattern with 300 hPa westerly zonal winds in the equatorial duct.

which facilitates interhemispheric mixing of trace gases. At other times, including El Niños, the u_{duct} are near zero or easterly, causing the Rossby wave eddies to be deflected northwards and dissipated in the equatorial regions, inhibiting interhemispheric exchange.

For the period July 2009 to June 2010, the average 300 hPa equatorial zonal winds in the duct region were easterly as shown in Fig. 4c, effectively closing the duct and increasing the build-up of FF CO_2 in the NH. The July 2008 to June 2009 open duct pattern, with westerlies in the duct, is shown in Fig. 4d. (Appendix C addresses the altitude range involved in this process. Note also, the meridional wind may make a small contribution to IH transport in the duct region during this time).

Figure 4b shows the 300 hPa zonal winds for July 2008 to June 2009 (Fig. 4d) minus those for July 2009 to June 2010 (Fig. 4c), and the pattern bears strong similarities with the long-term zonal wind versus SOI correlation in Fig. 4a.

5 Trace gas interhemispheric exchange through the duct

Interhemispheric exchange of a seasonally varying gas by this process depends on covariance with u_{duct} and is represented in Fig. 5 by the product of monthly u_{duct} and ΔC for routinely monitored CSIRO species C = CO_2, CH_4, CO, and H_2. The direction of a step in ΔC depends on the magnitude and sign of the trace gas IH gradient when the duct is open. The seasonality at mlo and cgo for the different gases is given in the Supplement.

In the top panel monthly u_{duct} is plotted over red and blue shading representing El Niño and La Niña periods respectively. We add symbols connected by a solid line that are an integration of the NH winter peaks, Σu_{duct} (October to April), for a nominal $u_{\mathrm{duct}} > 2\,\mathrm{m\,s^{-1}}$, in order to better compare year-to-year changes in the strength and duration of the seasonal duct exchange.

Figure 1 is re-examined in the light of variations in Σu_{duct}. Of the seven lowest Σu_{duct} in Fig. 5 – 1992, 1995, 1998, 2003, 2005, 2007, and 2010 – six correspond to peak $\Delta C_{\mathrm{mlo\text{-}cgo}}$ in CSIRO data. Differences between laboratories are more marked before the mid-1990s in Fig. 1a, marking a period of significant improvement in inter-laboratory quality monitoring (e.g. Masarie et al., 2001) but also influenced by the major perturbation to the carbon cycle associated with the 1991 Pinatubo eruption. However, the relationship with Σu_{duct} is, in the main, supported by SIO and NOAA data.

The two extreme cases of duct closure ($\Sigma u_{\mathrm{duct}} < 10\,\mathrm{m\,s^{-1}}$) since 1992 in Fig. 5 are in 1997–98 and 2009–10, showing up as a marked absence of a seasonal IH exchange ($\Delta C \times u_{\mathrm{duct}}$) for CO_2, CH_4, and CO. If the Fig. 1a ΔC step in 2009–10 is attributed to duct closure, then a similar ΔC change might be expected in 1997–98; however, it is less than half that in 2009–2010. The record CO_2 response to the 1997–

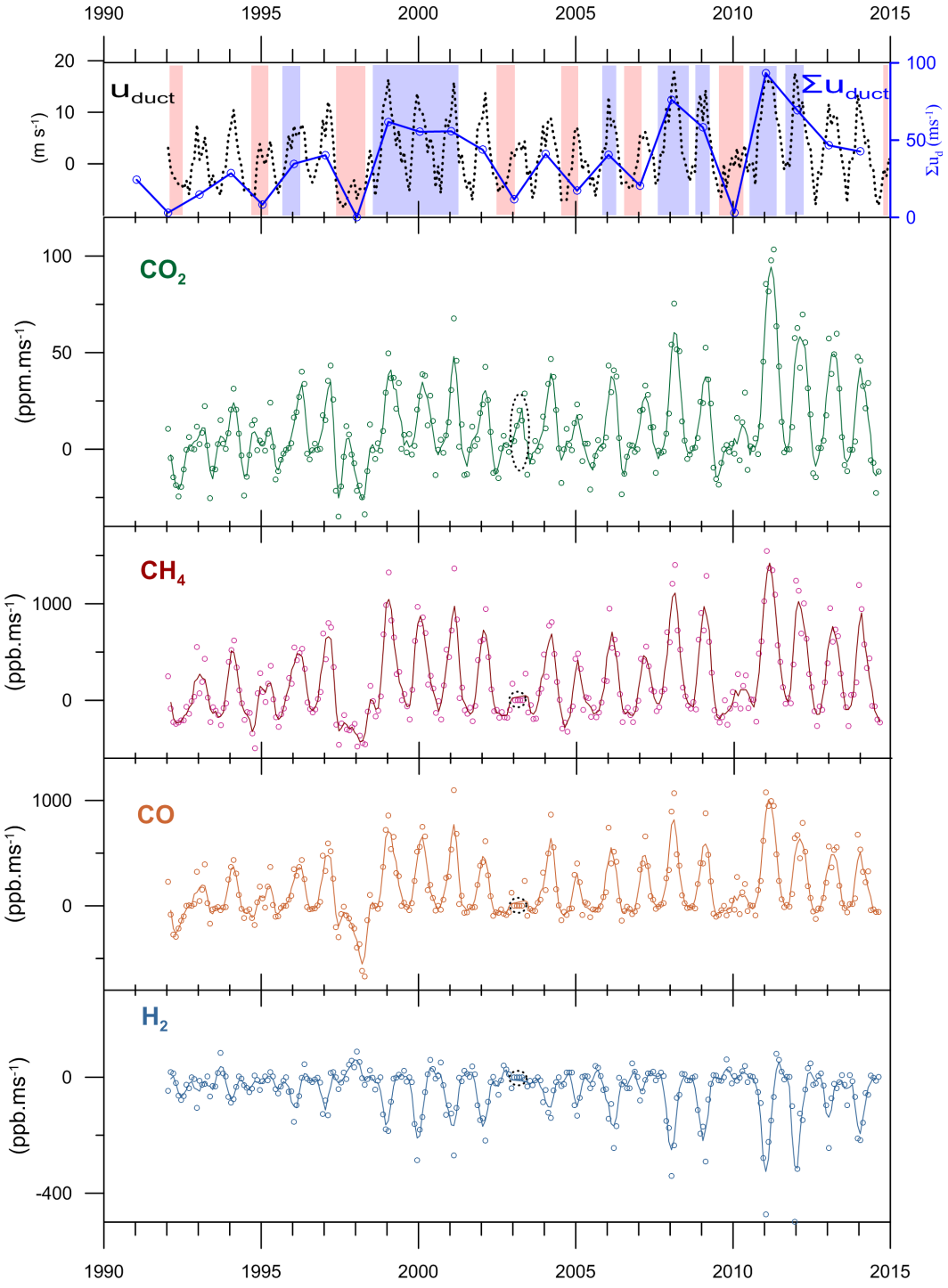

Figure 5. Monthly interhemispheric exchange for CSIRO trace gas species: the top panel shows monthly u_{duct} (300 hPa, 5° N to 5° S, 140 to 170° W), with red and blue bands indicating El Niño and La Niña periods respectively. The relative strength and duration of NH winter (October to April) IH mixing is estimated by Σu_{duct}, plotted in January. The following panels show the relative interhemispheric exchange fluxes ($\Delta C \times u_{\mathrm{duct}}$), due to Pacific upper-level equatorial turbulence, for different CSIRO flask species (CO_2, CH_4, CO, and H_2). Black circles indicate 4 months of missing CSIRO flask data from mlo; for CO_2, data from these months are obtained from NOAA records.

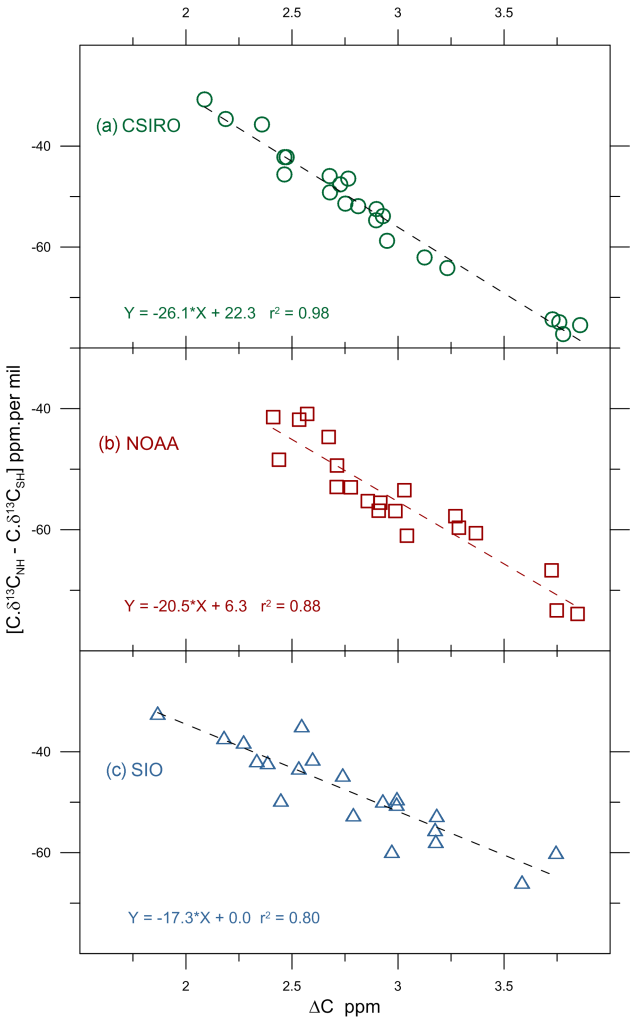

Figure 6. Isotopic evidence that interhemispheric CO_2 variations are systematic: the interhemispheric differences $\Delta^{13}CO_2$, represented by $\Delta(C \times \delta^{13}C)$ plotted against $\Delta^{12}CO_2$ for **(a)** CSIRO (mlo–cgo), **(b)** NOAA (mlo–cgo), and **(c)** SIO (mlo–spo) flask samples since 1992. (One 2003 NOAA outlier ($>5\sigma$), is removed from these plots and regressions.) The linear regression coefficients and correlation coefficients (r^2) are provided for each data set.

98 equatorial anomaly, associated with prolonged equatorial peat combustion (Sect. 3), is a possible explanation for a smaller response. The next lowest seasonally integrated $\Sigma u_{\text{duct}} \sim 10\,\text{m}\,\text{s}^{-1}$ in 2003 has the next largest ΔC increase in Figs. 1a and 2, strongly suggesting reduced seasonal IH transport. This complicates surface flux estimates from the inversion of CO_2 spatial differences by Rayner et al. (2008).

Switching focus to the positive excursions in Σu_{duct}, these are associated with increased strength of mixing through the open duct. Compared to previous behaviour, the magnitude of exchange ($\Delta C \times u_{\text{duct}}$) immediately after the extended duct closure from July 2009 to June 2010 is the largest for each gas in Fig. 5, in part reflecting the fact that the 2010–2011 La Niña corresponds to the most intense Σu_{duct} since 1990 (top panel Fig. 5). The unusual species exchange at this time is most marked for CO_2 and H_2, which we mainly attribute to the fact that these two gases exhibit the most significant ΔC trend (CO_2 positive, H_2 negative) over the 2 decades; also, each has seasonal concentration amplitudes that are the largest compared to mean annual IH gradients (Supplement).

Through the four "duct-open" periods after 2010, Fig. 1a shows ΔCO_2 to be practically constant, a phenomenon difficult to explain with known source and sink behaviour. During this period Σu_{duct} monotonically decreases; the constant ΔC might be explained if the decreasing Σu_{duct} is matched by decreases in the annual fossil fuel emission increments. Boden et al. (2013) estimate the annual increments in FF to be 0.5 Pg C in 2010, 0.3 Pg C in 2011, and 0.2 Pg C in 2012, supporting this interpretation.

6 Isotopic evidence of systematic ΔC variations

While covariance between atmospheric transport and terrestrial biosphere activity referred to as the "rectifier effect" is an important component in global carbon budgeting (Denning et al., 1999), it concerns seasonal variations in the depth of the atmospheric boundary layer rather than the abrupt upper-atmosphere transport through the duct described by Fig. 5.

Measurements of the stable carbon isotope in atmospheric CO_2 have the potential to clarify the relative importance of modes of atmospheric behaviour for ΔC. This depends on the fact that an atmospheric $^{13}CO_2$ anomaly is redistributed in the environment more rapidly than a $^{12}CO_2$ anomaly (Tans et al., 1993). This isotopic equilibration process is facilitated by the large gross turnover of CO_2 with oceanic and terrestrial reservoirs. It can reflect the time that has elapsed since an emission anomaly occurred and is examined below by comparing monthly with annually averaged data.

Measurements of the ratio of stable carbon isotopes, ^{13}C / ^{12}C, in atmospheric CO_2 are described by a reduced ratio $\delta^{13}C$ expressed in ‰; the ^{13}C content can be conveniently represented by the product $C \times \delta^{13}C$ (see Appendix B).

The dominant hemispheric CO_2 emissions are NH FF combustion and forest respiration. They each contain carbon that has undergone similar discrimination against the heavier isotope during photosynthesis. These sources are more depleted in ^{13}C content than other possible sources; for example, using Lloyd and Farquhar (1994) estimates of global discrimination relative to ambient atmospheric CO_2, forest carbon is globally ~ 18 ‰ lighter, savanna grasses are 4 ‰ lighter, and ocean carbon is in close equilibrium. (Note: -18 ‰ equals -1.8 %).

Despite having similar isotopic composition, the imprint of recent forest exchange and FF emissions on atmospheric $\delta^{13}C$ can be different. A convenient demonstration uses the direct monthly relationship between $\delta^{13}C$ and C (only valid

over small ranges of C), which in the NH is characterized by $-0.05\,‰\,\mathrm{ppm}^{-1}$ and, since the seasonal variation in the SH is small, this relationship exists for monthly NH-SH $\Delta\delta^{13}C$. On annual timescales the C and $\delta^{13}C$ seasonal variations are largely cancelled, with negligible contribution to IH differences, and ΔC changes are dominated by the steadily accumulating NH FF emissions that have greater opportunity for isotopic equilibration, which is evidenced over the last 2 decades by the observed mlo–cgo annual average $\Delta\delta^{13}C$ / ΔC of $-0.027 \pm 0.003\,‰\,\mathrm{ppm}^{-1}$.

Significant in the present context, however, over the limited excursion range of annually averaged CSIRO pre-2010 data NH–SH $\Delta\delta^{13}C = -0.050(\pm 0.004)\Delta C + 0.062\,‰$ ($r^2 = 0.92$), identical to the monthly covariations in $\Delta\delta^{13}C$ and suggesting involvement of unequilibrated forest CO_2.

Francey et al. (2013) reported a synchronous decrease in stable carbon isotope ratio at the time of the 2009–2010 ΔCO_2 increase, measured in the same flask air samples. Those data are updated in Fig. 6 and provided in the Supplement.

Figure 6 plots the relative IH spatial changes in ^{13}C, represented by $C \times \delta^{13}C_{NH}$-$C \times \delta^{13}C_{SH}$, compared to those in ^{12}C (using $C_{NH\text{-}SH}$, since C is 99 % ^{12}C) in the CSIRO, NOAA, and SIO samples used in Fig. 1a. All three data sets, and particularly CSIRO, show a linear relationship including the pre-2010 scatter, the 2009–2010 step, and subsequent data. The slope of the linear regressions represents the sum of source discrimination and ambient atmospheric $\delta^{13}C$ (Enting et al., 1993; Enting, 2006).

Thus, with the Lloyd and Farquhar estimate of global forest discrimination of $-18\,‰$ and an atmospheric value of $-8\,‰$ (e.g. the seasonal minimum at mlo in 2009–10), the $-26.1\,‰$ slope for the CSIRO data is near the most negative anticipated value, excluding significant influences of other possible CO_2 sources, such as savanna grasses, and excluding significant isotopic equilibrations that occur on longer than seasonal timescales, all of which result in less negative slopes. These data strongly favour a major role for the duct transfer mechanism, for both the step and prior variability, since it occurs close to the seasonal CO_2 peak ($\delta^{13}C$ minimum) of NH terrestrial biosphere respiration in Fig. 5.

The relationship is far less well-defined in the NOAA and SIO data with regression slopes of -20 and $-17\,‰$, which, while both favouring C3 sources, do not exclude significant contributions from other sources, including annually distributed, equilibrated FF CO_2. Note, however, that if the 2009–2010 step was due to savanna grasses, then the post-2010 points (to the far right) in Fig. 6 would not fit on the 2-decade regressions of any of the three data sets, since the anticipated slope for savanna exchange is around $-12\,‰$.

The NOAA and SIO data exhibit more scatter, with linear regression residual mean square scatter of 5, 11, and 17 ppm per mil for CSIRO, NOAA, and SIO plots respectively. A lack of correlation in $\Delta\delta^{13}C$ variations between the NOAA and SIO suggests that, whatever the IH transport mechanism, isotopic measurement precision is a more limiting factor in these data sets. By comparison, as befits an SH focus, precision has been a greater concern in CSIRO measurement programs, resulting in extensive published quality control assessments of the CSIRO isotope data since 1992, described in Appendix B, and supporting our preference for these data.

The intermittent nature of this IH exchange process might be expected to show up in other species like SF_6, used by the modelling community to diagnose IH transport (Patra, 2015). We address this issue in Appendix C. Incidentally, the estimate of possible covariance between $\delta^{13}C$ and gross terrestrial primary productivity (Randerson et al., 2002) is likely to be impacted if a significant portion of IH exchange is via the upper-atmosphere equatorial duct.

7 Historic evidence for anomalous interhemispheric CO_2 exchange

Figure 7 examines the historic SIO mlo–spo records (Keeling et al., 2009) for responses to five other extended periods of duct closure since the 1960s. Working backwards in time, there are seven occasions (circled in the top panel) when the seasonal $\Sigma u_{duct} < 5\,\mathrm{m\,s}^{-1}$. The five of these that correspond to an El Niño period closely followed by a La Niña (or in the case of 1982–1983, a weak La Niña shortly followed by a stronger one) show prominent peak values in ΔC (circled bottom panel); the two low Σu_{duct} not coinciding with a ΔC peak (smaller circles) have relatively brief El Niño periods not followed by La Niña. While there are two small ΔC peaks prior to 1970, the ΔC are more susceptible to missing data (particularly at spo) and measurement bias (Francey et al., 2016), and NCEP data may be less reliable, so are not considered further here. The 1986–88 event most mirrors 2009–10, being the next largest step, followed by 4 years of relatively stable ΔC.

We conclude from this that anomalies in the interhemispheric exchange through the duct have played a significant ongoing role in modifying spatial differences in CO_2 (and other trace species) at the surface. As NH FF CO_2 emissions increase further, the influence is expected to become more marked in $\Delta C \times u_{duct}$.

8 Conclusions

Peylin et al. (2013) describe conflict between groups of carbon budgeting models in locating the major global terrestrial sink, whether mid-northern latitude or equatorial, and suggest that atmospheric transport implementations may be involved. We have presented a variety of complementary evidence, including CO_2 isotopes, linking interhemispheric transport through the Pacific upper-troposphere equatorial duct and the spatial and temporal difference in measured surface CO_2 concentrations. The observed patterns of CO_2 interhemispheric changes are not easily explained by observed

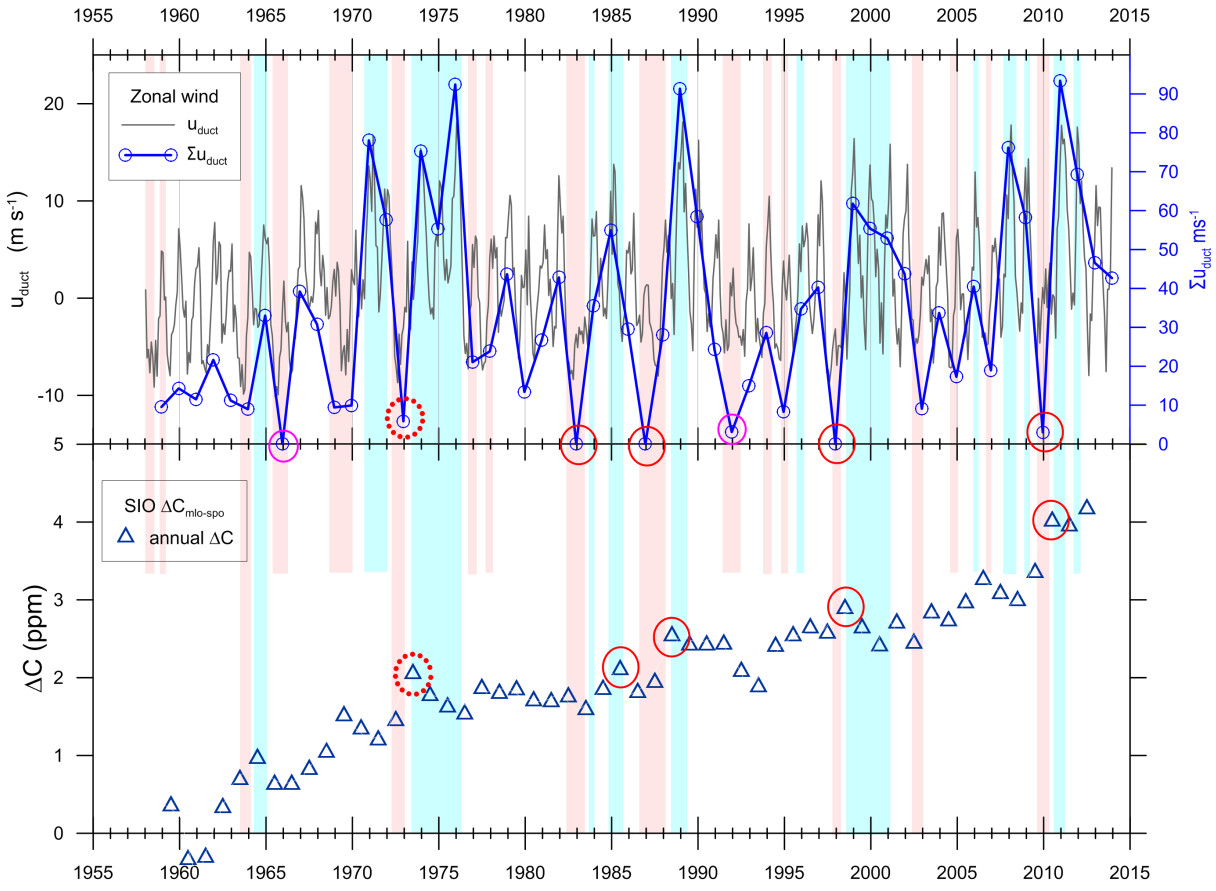

Figure 7. Interhemispheric mlo–spo differences from the historic Keeling CO_2 record and u_{duct}: the top panel shows monthly u_{duct} (300 hPa, 5° N to 5° S, 140 to 170° W), with red and blue bands indicating El Niño and La Niña periods respectively (left axis). The relative strength and duration of NH winter (October to April) IH mixing is estimated by Σu_{duct}, plotted in January (right axis). In the bottom panel annual average mlo–spo ΔC are shown. Red circles indicate occasions when integrated duct transport is $< 5\,m\,s^{-1}$, dashed for $> 5\,m\,s^{-1}$, and smaller circles (in the top panel) indicate occasions when brief closures are not followed by La Niña and there is no detectable ΔC influence.

source and sink behaviour. If the parameterizations of transport in the global carbon budget models do not adequately capture the duct process, then spatial differences arising from transport are most likely to be interpreted as variation in terrestrial sinks. It also suggests that the SH seasonality in CO_2 may have been misinterpreted. For example, when the duct is open, the January to April IH exchange through the duct will offset the spring minimum CO_2 level due to SH terrestrial uptake. The conventional explanation has a ∼ 6-month delayed exchange arriving in the SH autumn and enhancing peak SH respiration. Global budgeting of other trace gas studies (e.g. Locatelli et al., 2013) is also likely to be impacted.

The observed 2009–2010 changes in CO_2 IH difference in particular, because of the magnitude and also the absence of plausible reported source and sink changes (in a time of unprecedented monitoring of ecosystem and ocean exchanges), provide an unusual opportunity to test the implementation of atmospheric transport in inversion models and help remove current ambiguities between surface exchanges and transport. More generally, this requires such models to demonstrate an ability to describe the spatial and temporal systematic differences in selected high-quality baseline trace gas records that have well-established large-scale representation, such as the mlo–cgo records used here.

Appendix A: Trace gas data processing

The analyses for both dC/dt and ΔC are based on monthly average mixing ratios (or $\delta^{13}C$ isotopic ratios) obtained from a smooth curve through individual flask data (typically four per month) with a combined harmonic (seasonal) and 80-day smoothing spline (Thoning et al., 1989). At Cape Grim, selected data represent strong near-surface winds ($>5\,m\,s^{-1}$; 164 m a.s.l.) with trajectories (typically > 10 days) over the Southern Ocean; at Mauna Loa samples are collected in moderate downslope winds; South Pole samples are selected to avoid local (station) contamination. Conventional smoothing splines through deseasonalized baseline-selected concentration data, with 50 % attenuation at 22 months, are differentiated to provide dC/dt since 1992; Francey et al. (2016) discuss dC/dt uncertainties. Annually averaged ~ 80-day smoothed monthly baseline concentration data are used to provide ΔC with near-annual time resolution, i.e. potential ambiguity between seasonality and interannual variation is addressed differently by dC/dt and ΔC. CSIRO and NOAA data are processed identically. Scripps atmospheric CO_2 data used here are monthly data that are seasonally adjusted and filled (http://scrippsco2.ucsd.edu/).

(Note: using the spatial differences from individual laboratories effectively removes most calibration issues that can complicate high-precision comparisons of data between laboratories).

Appendix B: Laboratory differences in $\delta^{13}C$ data

The $\delta^{13}C$ in CO_2 are a "reduced ratio" of ^{13}C / ^{12}C, for sample s and reference r:

$$\delta^{13}C_s = \left({}^{13}C_s/{}^{12}C_s - {}^{13}C_r/{}^{12}C_r\right) / \left({}^{13}C_r/{}^{12}C_r\right). \quad \text{(B1)}$$

Mass conservation in ^{13}C is approximated using the product of C and $\delta^{13}C$ (e.g. Tans et al., 1993).

The assumption of independence between C and $\delta^{13}C$ measurements is marginally compromised by the use of the N_2O / CO_2 ratio to correct the $\delta^{13}C$ for mass spectrometer split resolution (e.g. Allison and Francey, 2007). The difference in 2009 and 2010 corrections to $\Delta\delta^{13}C$ is < 0.0007 ‰ compared with the magnitude of ~ 0.029 ‰ for the 2009–2010 step (C. Allison, personal communication, 2015).

Flask CO_2 differences between NOAA and CSIRO same-air comparisons at cgo since 1992 are 0.11 ± 0.13 ppm (Masarie et al., 2001; Francey et al., 2016). It is assumed that the mean offset cancels when using mlo–cgo differences. This implies that the maximum $\delta^{13}C$ measurement error due to flask air contamination should be less than 0.005 ‰.

Exact reasons for the varying quality of $\delta^{13}C$ programs in Fig. 6 are not known. However, reduced scatter in the CSIRO program is possibly related to feedback from regular quality assessment provided by unique method redundancy (Allison and Francey, 2007). The data in this report involve small subsamples of chemically dried whole-flask air, from which CO_2 is extracted and analysed using a fully automated Finnigan MAT 602 D mass spectrometer (MS) with MT Box-C extraction accessory and bracketed by extractions and analysis of cgo long-lived baseline air standards in high-pressure cylinders. Over most of the 2 decades, a parallel cgo program involved unique large-sample in situ extraction of CO_2, which is returned and analysed on the same MS but relative to independently propagated pure CO_2 standards.

Despite inadequate support to maintain future quality control in the CSIRO isotope program, a 2013 thorough quality audit occurred in the context of comparing recent and 1990s $\delta^{13}C$ measurements of ice core air (Rubino et al., 2013).

Appendix C: Atmospheric transport

In contrast to the situation in Fig. 4c, the average 300 hPa zonal wind for July 2008 to June 2009, shown in Fig. 4d, has equatorial westerlies between the date line and 120° W. The westerly duct is open and NH extratropical Rossby waves, including the Himalayan wave train, are able to penetrate into the SH. Correlation analysis (Frederiksen and Webster, 1988) indicates increased upper-tropospheric transient kinetic energy near the Equator with facilitated IH transport of trace gases. Here we have focused on the 300 hPa level, but our results apply in broad terms to most of the upper troposphere. In particular, the correlation of the SOI with the zonal wind in the westerly duct region (Fig. 4a) applies between 500 and 70 hPa, with similar strength between 300 and 100 hPa and reducing at the upper and lower levels. Again, the structure of the zonal wind differences of July 2008–June 2009 minus July 2009–June 2010 (Fig. 4b) is largely equivalent barotropically, with similar strength between 300 and 100 hPa and reducing at the upper and lower levels. Northern winter (DJF) differences for 2008–2009 minus 2009–2010 are circa twice as strong in the westerly duct region as in Fig. 4b.

The Patra atmospheric transport modelling (Patra, 2015) relies on measurements of SF_6 to support the transport parameterization. Our early examination of such synthetic species with respect to the 2009–2010 event was inconclusive. While we can demonstrate a considerable degree of systematic behaviour in the variation in baseline monthly CO_2 IH differences, by comparison the synthetics were found to have much larger scatter, though significant precision improvements have occurred since 2011 (Paul Krummel, personal communication, 2015). Furthermore, over the period of most concern, we found little agreement between the NOAA HATS SF_6 data (http://www.esrl.noaa.gov/gmd/hats/combined/SF6.html) and equivalent data from the AGAGE network (https://agage.mit.edu/) in month-to-month or interannual variability about the long-term increase in IH difference. The use of past SF_6 to calibrate the interhemispheric transport may well be adequate for the long-term model mean transport but fail to adequately constrain past irregular periods such as 2009–2010 or similar historic events.

The Supplement related to this article is available online at doi:10.5194/bg-13-873-2016-supplement.

Author contributions. R. J. Francey proposed this study and provided trace gas information, and J. S. Frederiksen provided the atmospheric dynamics information.

Acknowledgements. We are grateful to Anonymous Referee no. 1, Prabir Patra, and Ben Poulter for their constructive criticism of the discussion paper. The paper relies on the decades-long commitment by skilled CSIRO GASLAB scientific personnel, particularly Paul Steele, Ray Langenfelds, Paul Krummel, Colin Allison, Paul Fraser, and Marcel van der Schoot. Many support staff in GASLAB, Cape Grim Baseline Air Pollution Station (The Australian Bureau of Meteorology with CSIRO), and measurement collaborators at NOAA also contribute directly in this regard. The importance of the historic SIO records cannot be overstated. Rachel Law provided global, and Ying Ping Wang with Chris Lu regional, CO_2 modelling advice. Ian Enting provided guidance on interpreting the $\delta^{13}C$ spatial gradients.

Edited by: S. Zaehle

References

Allison, C. E. and Francey, R. J.: Verifying southern hemisphere trends in atmospheric carbon dioxide stable isotopes, J. Geophys. Res., 112, D21304, doi:10.1029/2006JD007345, 2007.

Ashfold, M. J., Pyle, J. A., Robinson, A. D., Meneguz, E., Nadzir, M. S. M., Phang, S. M., Samah, A. A., Ong, S., Ung, H. E., Peng, L. K., Yong, S. E., and Harris, N. R. P.: Rapid transport of East Asian pollution to the deep tropics, Atmos. Chem. Phys., 15, 3565–3573, doi:10.5194/acp-15-3565-2015, 2015.

Boden, T. A., Marland, G., and Andres, R. J.: Global, regional, and national fossil-fuel CO_2 emissions, Carbon Dioxide Information Analysis Center, 2013.

Ciais, Ph., Reichstein, M., Viovy, N., Granier, A., Ogée, J., Allard, V., Aubinet, M., Buchmann, N., Bernhofer, Chr., Carrara, A., Chevallier, F., De Noblet, N., Friend, A. D., Friedlingstein, P., Gr?nwald, T., Heinesch, B., Keronen, P., Knohl, A., Krinner, G., Loustau, D., Manca, G., Matteucci, G., Miglietta, F., Ourcival, J. M., Papale, D., Pilegaard, K., Rambal, S., Seufert, G., Soussana, J. F., Sanz, M. J., Schulze, E. D., Vesala, T., and Valentini, R.: Europe-wide reduction in primary productivity caused by the heat and drought in 2003, Nature, 437, 529–533, doi:10.1038/nature03972, 2005.

Denning, A. S., Takahashi, T., and Friedlingstein, P: Can a strong atmospheric CO_2 rectifier effect be reconciled with a "reasonable" carbon budget? Tellus, 51B, 249–253, 1999.

Dlugokencky, E. J., Lang, P. M., Masarie, K. A., Crotwell, A. M., and Crotwell, M. J.: Atmospheric Carbon Dioxide Dry Air Mole Fractions from the NOAA ESRL Carbon Cycle Cooperative Global Air Sampling Network, 1968–2013, Version: 2014-06-27, 2014.

Enting, I. G.: Inverse Problems in Atmospheric Constituent Transport, Cambridge Univesity Press, 0521812100, 2006.

Enting, I. G., Trudinger, C. M., Francey, R. J., and Granek, H.: Synthesis inversion of atmospheric CO_2 using the GISS tracer transport model. CSIRO Division of Atmospheric Research Technical Paper No. 29, 551.51120287, CSIRO Australia, 1993.

Francey, R. J., Trudinger, C. M., van der Schoot, M., Law, R. M., Krummel, P. B., Langenfelds, R. L., Steele, L. P., Allison, C. E., Stavert, A. R., Andres, R. J., and Rödenbeck, C.: Atmospheric verification of anthropogenic CO_2 emission trends, Nature Climate Change, 3, 520–524, doi:10/1038/nclimate1817, 2013.

Francey, R. J., Langenfelds, R. L., Steele, L. P., Krummel, P. B., and van der Schoot, M.: Bias in the biggest terms in the global carbon budget?, in: Baseline Atmospheric Program Australia 2011–2013, edited by: Krummel, P. B. and Derek, N., Melbourne, Australian Bureau of Meteorology in cooperation with CSIRO Division of Atmospheric Research, in press, 2016.

Frederiksen, J. S. and Webster, P. J.: Alternative theories of atmospheric teleconnections and low-frequency fluctuations, Rev. Geophys., 26, 459–494, 1988.

Giglio, L., Randerson, J. T., and van derWerf, G. R.: Analysis of daily, monthly, and annual burned area using the fourth-generation global fire emissions database (GFED4), J. Geophys. Res.-Biogeo., 118, 317–328, doi:10.1002/jgrg.20042, 2013.

Keeling, R. F., Piper, S. C., Bollenbacher, A. F., and Walker, J. S.: Atmospheric CO_2 records from sites in the SIO air sampling network. In Trends: A Compendium of Data on Global Change. Carbon Dioxide Information Analysis Center, Oak Ridge National Laboratory, U.S. Department of Energy, Oak Ridge, Tenn., USA, doi:10.3334/CDIAC/atg.035, 2009.

Law, R. M.: The Community Atmosphere Land Exchange (CABLE) model: results from ACCESS1.3 and new simulations with CABLE-2.0, http://www.climatescience.org.au/sites/default/files/LAW_COECSS_Sep2012.pdf (last access: January 2016), 2014.

Law, R. M., Kowalczyk, E. A., and Wang, Y.-P.: Using atmospheric CO_2 data to assess a simplified carbon-climate simulation by for the 20th century, Tellus, 58B, 427–437, 2006.

Lloyd, J. and Farquhar, G. D.: ^{13}C discrimination during CO_2 assimilation by the terrestrial biosphere, Oecologia, 99, 201–215, 1994.

Locatelli, R., Bousquet, P., Chevallier, F., Fortems-Cheney, A., Szopa, S., Saunois, M., Agusti-Panareda, A., Bergmann, D., Bian, H., Cameron-Smith, P., Chipperfield, M. P., Gloor, E., Houweling, S., Kawa, S. R., Krol, M., Patra, P. K., Prinn, R. G., Rigby, M., Saito, R., and Wilson, C.: Impact of transport model errors on the global and regional methane emissions estimated by inverse modelling, Atmos. Chem. Phys., 13, 9917–9937, doi:10.5194/acp-13-9917-2013, 2013.

Masarie, K. A., Langenfelds, R. L., Allison, C. E., Conway, T. J., Dlugokencky, E. J., Francey, R. J., Novelli, P. C., Steele L. P., Tans P. P., Vaughn B., and White, J. W. C.: NOAA/CSIRO Flask Air Intercomparison Experiment: A strategy for directly assessing consistency among atmospheric measurements made by independent laboratories. J. Geophys. Res., 106, 20445–20464, 2001.

Matsueda, H., Machida, T., Sawa, Y., and Niwa, Y.: Long-term change of CO_2 latitudinal distribution in the upper troposphere, Geophys. Res. Lett., 42, 2508–2514, doi:10.1002/2014GL062768, 2015.

McGregor, J. L. and Dix, M. R.: An updated description of the conformal-cubic atmospheric mode, in: High Resolution Simulation of the Atmosphere and Ocean, edited by: Hamilton, K. and Ohfuchi, W., Springer, 51–76, 2008.

Miyazaki, K., Patra, P. K., Takigawa, M., Iwasaki, T., and Nakazawa, T.: Global-scale transport of carbon dioxide in the troposphere, J. Geophys. Res., 113, D15301, doi:10.1029/2007JD009557, 2008.

Page, S. E., Hoscilo, A., Langner, A., Tansey, K. J., Siegert, F., Limin, S. H., and Rieley, J. O.: Tropical peatland fires in Southeast Asia, in: Tropical Fire Ecology: Climate Change, Land Use and Ecosystem Dynamics, edited by: Cochrane, M. A., Springer-Praxis, Heidelberg, Germany, 263–287, 2009.

Patra, P.: Interactive comment on "The 2009–2010 step in atmospheric CO_2 inter-hemispheric difference" by R. J. Francey and J. S. Frederiksen, Biogeosciences Discuss., 12, C6469–C6469, 2015.

Peters, G. P., Marland, G., Le Quéré, C., Boden, T., Canadell, J. G., and Raupach, M. R.: Rapid growth in CO_2 emissions after the 2008–2009 global financial crisis, Nature Climate Change, 2, 1–4, doi:10.1038/nclimate1332, 2012.

Peylin, P., Law, R. M., Gurney, K. R., Chevallier, F., Jacobson, A. R., Maki, T., Niwa, Y., Patra, P. K., Peters, W., Rayner, P. J., Rödenbeck, C., van der Laan-Luijkx, I. T., and Zhang, X.: Global atmospheric carbon budget: results from an ensemble of atmospheric CO_2 inversions, Biogeosciences, 10, 6699–6720, doi:10.5194/bg-10-6699-2013, 2013.

Poulter, B.: Interactive comment on "The 2009–2010 step in atmospheric CO_2 inter-hemispheric difference" by R. J. Francey and J. S. Frederiksen, Biogeosciences Discuss., 12, C7009–C7011, 2015.

Poulter, B., Frank, D., Ciais, P., Myneni, R. B., Andela, N., Bi, J., Broquet, G., Canadell, J. G., Chevallier, F., Liu, Yi Y., Running, S. W., Sitch, S., and van der Werf, G. R.: Contribution of semi-arid ecosystems to inter-annual variability of the global carbon cycle, Nature, 509, 600–603, doi:10.1038/nature13376, 2014.

Rayner, P. J., Law, R. M., Allison, C. E., Francey, R. J., Trudinger, C. M., and Pickett-Heaps, C.: Interannual variability of the global carbon cycle (1992–2005) inferred by inversion of atmospheric CO_2 and $\delta^{13}CO_2$ measurements, Global Biogeochem. Cy., 22, GB3008, doi:10.1029/2007GB003068, 2008.

Randerson, J. T., Collatz, G. J., Fessenden, J. E., Munoz, A. D., Still, C. J., Berry, J. A., Fung, I. Y., Suits, N., and Denning, A. S.: A possible global covariance between terrestrial gross primary production and ^{13}C discrimination: Consequences for the atmospheric ^{13}C budget and its response to ENSO, Global Biogeochem. Cy., 16, 1136–1152, doi:10.1029/2001GB001845, 2002.

Rubino, M., Etheridge, D. M., Trudinger, C. M., Allison, C. E., Battle, M. O., Langenfelds, R. L., Steele, Curran, M., Bender, M., White, J. W. C., Jenk, T. M., Blunier, T., and Francey, R. J.: A revised 1000 year atmospheric $\delta^{13}C$-CO_2 record from Law Dome and South Pole, Antarctica, J. Geophys. Res. 118, doi:10.1002/jgrd.50668, 2013.

Stephens, B. B., Gurney, K. R., Tans, P. P., Sweeney, C. Peters, W., Bruhwiler, L., Ciais, P., Ramonet, M., Bousquet, P., Nakazawa, T., Aoki, S., Machida, T., Inoue, G., Vinnichenko, N., Lloyd, J., Jordan, A., Heimann, M., Shibistova, O., Langenfelds, R. L. Steele, L. P., Francey, R. J., and Denning, A. S.: The vertical distribution of atmospheric CO_2 defines the latitudinal partitioning of global carbon fluxes, Science, 316, 1732–1735, 2007.

Stephens, B. B., Brailsford, G. W., Gomez, A. J., Riedel, K., Mikaloff Fletcher, S. E., Nichol, S., and Manning, M.: Analysis of a 39-year continuous atmospheric CO_2 record from Baring Head, New Zealand, Biogeosciences, 10, 2683–2697, doi:10.5194/bg-10-2683-2013, 2013.

Tans, P. P., Berry, J. A., and Keeling, R. F.: Oceanic ^{13}C data: A new window on CO_2 uptake by the oceans, Global Biogeochem. Cy., 7, 353–368, 1993.

Thoning, K. W., Tans, P. P., and Komhyr, W. D.: Atmospheric carbon dioxide at Mauna Loa observatory, 2, Analysis of the NOAA/GMCC data, 1974–1985, J. Geophys. Res., 94, 8549–8565, 1989.

Webster, P. J. and Holton, J. R.: Cross-equatorial response to mid-latitude forcing in a zonally varying basic state, J. Atmos. Sci., 39, 722–733, 1982.

Webster, P. J. and Chang, H.-R.: Equatorial energy accumulation and emanation regions: Impacts of a zonally varying basic state, J. Atmos. Sci., 45, 803–829, 1988.